Inorganic Chemistry

Article

Cite This: Inorg. Chem. XXXX, XXX, XXX–XXX

pubs.acs.org/IC

Effects of Thiolate Ligation in Monoiron Hydrogenase (Hmd): Stability of the $\{Fe(CO)_2\}^{2+}$ Core with NNS Ligands

Zhu-Lin Xie, Doran L. Pennington, Dylan G. Boucher, James Lo, and Michael J. Rose*

Department of Chemistry, The University of Texas at Austin, Austin, Texas 78712, United States

Supporting Information

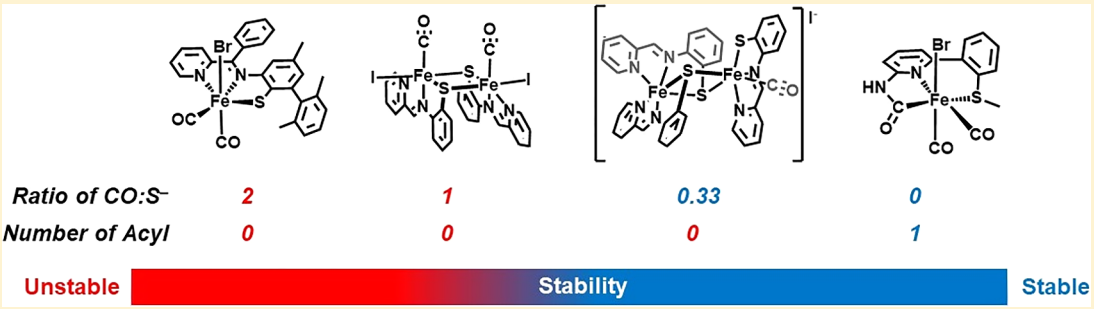

ABSTRACT: In this work, we report the effects of NNS-thiolate ligands and nuclearity (monomer, dimer) on the stability of iron complexes related to the active site of monoiron hydrogenase (Hmd). A thermally stable iron(II) dicarbonyl motif is the core feature of the active site, but the coordination features that lead to this property have not been independently evaluated for their contributions to the $\{Fe(CO)_2\}^{2+}$ stability. As such, non-bulky and bulky benzothiazoline ligands (thiolate precursors) were synthesized and their iron(II) complexes characterized. The use of non-bulky thiolate ligands and low-temperature crystallizations result in isolation of the dimeric species $[(NNS)_2Fe_2(CO)_2(I)_2]$ (**1**), $[(N^{Ph}NS)_2Fe_2(CO)_2(I)_2]$ (**2**), and $[(^{Me}NNS)_2Fe_2(CO)_2(I)_2]$ (**3**), which exhibit dimerization via thiolato $(\mu_2\text{-}S)_2$ bridges. In one particular case (unsubstituted NNS ligand), the pathway of decarbonylation and oxidation from **1** was crystallographically elucidated, via isolation of the half-bis-ligated monocarbonyl dimer $[(NNS)_3Fe_2(CO)]I$ (**4**) and the fully decarbonylated and oxidized mononuclear $[(NNS)_2Fe]I$ (**5**). The transformations of dicarbonyl complexes (**1**, **2**, and **3**) to monocarbonyl complexes (**4**, **6**, and **7**) were monitored by UV/vis, demonstrating that **1** and **3** exhibit longer $t_{1/2}$ (80 and 75 min, respectively) than **2** (30 min), which is attributed to distortion of the ligand backbone. Density functional theory calculations of isolated complexes and putative intermediates were used to corroborate the experimentally observed IR spectra. Finally, dimerization was prevented using a bulky ligand featuring a 2,6-dimethylphenyl substituent, which affords mononuclear iron dicarbonyl complex, $[(N^{Ph}NS^{DMPh})Fe(CO)_2Br]$ (**8**), identified by IR and NMR spectroscopies. The dicarbonyl complex decomposes to the decarbonylated $[(N^{Ph}NS^{DMPh})_2Fe]$ (**9**) within minutes at room temperature. Overall, the work herein demonstrates that the thiolate moiety does not impart thermal stability to the $\{Fe(CO)_2\}^{2+}$ unit formed in the active site, further indicating the importance of the organometallic Fe-C(acyl) bond in the enzyme.

INTRODUCTION

As the depletion of fossil fuels approaches and the need for renewable energy sources increases, attention has turned to the production and utilization of dihydrogen (H_2).[1−3] The development of biomimetic catalysts that efficiently perform H_2-related reactions, such as H_2 activation and water oxidation, are of particular interest. Nature has developed three types of hydrogenases that activate and utilize H_2 using different mechanisms. These enzymes include [FeFe], [FeNi], and the most recently discovered mono-[Fe] hydrogenase (also called hydrogen-forming methylene-tetrahydromethanopterin dehydrogenase (Hmd)), which is endogenously expressed in methanogens such as *Methanocaldococcus jannaschii*.[4−6] The unique feature of the mono-[Fe] hydrogenase is that it catalyzes the heterolytical splitting of H_2 and produces H^+ and H^-, the latter of which is transferred to the substrate, methenyltetrahydromethanopterin (H_4MPT^+, Scheme 1). This H_2 cleavage and hydride transfer by

Scheme 1. Reaction Catalyzed by Hmd

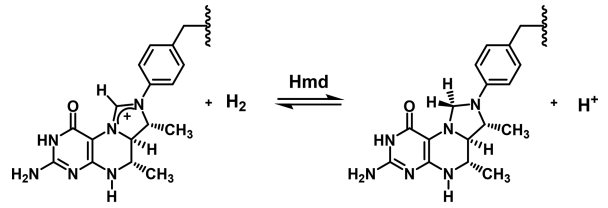

[Fe] hydrogenase is an intermediate step in the methanogenic reduction of CO_2 to CH_4, where H_4MPT^+ serves as a C_1 carrier in the metabolic cycle.[4−6]

Received: April 30, 2018

DOI: 10.1021/acs.inorgchem.8b01185
Inorg. Chem. XXXX, XXX, XXX–XXX

The structure of the active site of Hmd was determined crystallographically by Shima and co-workers.[7,8] As shown in Scheme 2, the active site contains an Fe(II) ion ligated by a

Scheme 2. Active Site of Hmd Detailing the Two Possible Protonation States: Pyridinol (left) versus Pyridone (right)

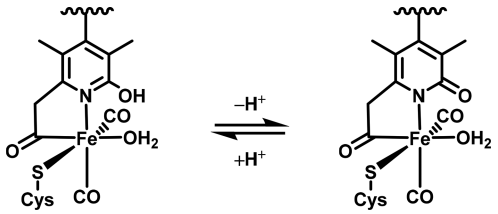

bidentate acyl-pyridone/pyridinol ligand, two terminal CO groups in cis orientation, and a cysteinyl sulfur (Cys176). The coordination site trans to the acyl unit is occupied by solvent (H_2O) in its resting state and is the putative binding and activation site for H_2. Although the exact mechanism of H_2 activation remains unknown, researchers agree that either the pyridone oxygen or cysteine sulfur serves as the "pendant base" in cooperation with the Lewis acidic Fe(II) ion.[9−11] As a result, the kinetic barrier of H_2 cleavage has been calculated to be drastically lowered ($\Delta G^{\ddagger} \approx 2$ kcal/mol).[11]

One seemingly innocuous feature of the active site warrants some discussion: the *cis*-$\{Fe(CO)_2\}^{2+}$ motif. While hundreds of examples of structurally characterized iron(II) carbonyl complexes can be found in the Cambridge Crystallographic Data Centre (CCDC), there are relatively few *phosphine-free* coordination complexes containing *cis*-$\{Fe(CO)_2\}^{2+}$ motif.

More specific to the enzyme, synthetic models of [Fe]-hydrogenase have been developed to understand the mechanistic details, reactivity, and bonding of the active site. Previously, Hu and co-workers reported a series of methylene-acyl containing iron complexes exhibiting structural relevance to the Hmd active site (Scheme 3).[12] Pickett and co-workers

Scheme 3. Synthetic Models for [Fe] Hydrogenase

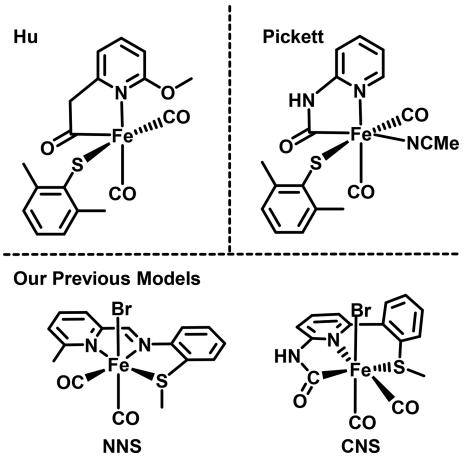

synthesized a series of "carbamoyl" (amide-acyl) iron complexes that mimicked the active site. And while the aforementioned models replicated most features of the first coordination sphere, none exhibited the enzyme-like functionality of H_2 cleavage in the absence of the protein environment.[13]

Previously, we utilized Schiff base (NNS) and carbamoyl-pincer (CNS) ligands bearing thioether moieties to generate mononuclear iron(II) carbonyl species resembling the active site to lesser or greater extents, respectively (Scheme 3).[14−16] While both systems replicated the *cis*-$\{Fe(CO)_2\}^{2+}$ motif, the Schiff base ligand did not provide thermal stability (decarbonylation occurred above −20 °C in coordinating solvent), and the pincer−CNS complex—while stable up to 50 °C in coordinating solvents—did not exhibit any reactivity with H_2 or model substrates. In fact, in the latter case (pincer), CO dissociation was only observed when using a strong decarbonylation reagent such as Me_3NO.[16] Overall, on these premises, it was not clear whether the inclusion of a thiolate donor (in the absence of an acyl-C donor) would provide (i) thermal stability to the *cis*-$\{Fe(CO)_2\}^{2+}$ unit, or (ii) promote reactivity with H_2 and model substrates. Therefore, in this work we incorporated a thiolate into the donor set to evaluate its structural preferences and thermal stability. One possible outcome of thiolate metalation ligands is the formation of dimeric or multinuclear complexes due to the bridging tendency of thiolato-S (Scheme 4). By increasing the bulkiness of

Scheme 4. Targeted Ligands and Dicarbonyl Complex

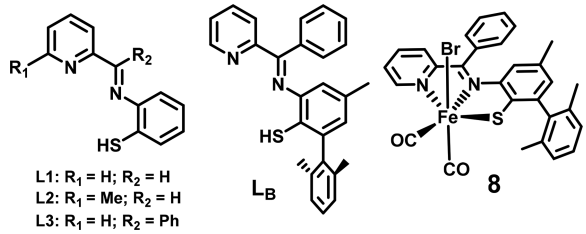

the thiolate, we attempted to avoid the bridging thiolate motif and thus afford mononuclear complex, as we demonstrated in our anthracene-base CNS(thiolate) model.[17] Herein, we report the synthesis of Schiff base thiolate iron complexes and, ultimately, control of nuclearity of these complexes by varying the steric hindrance of the thiolate ligands.

RESULTS AND DISCUSSION

Syntheses. *Non-bulky Ligands.* The non-bulky ligands were derived from condensation of the substituted pyridine carboxaldehyde or ketone with 2-aminobenzenethiol, based on the literature report (Scheme 5).[18,19] The thermodynamically more favorable benzothiazoline products were obtained as a result of cyclization after condensation (Scheme 5), wherein the benzothiazoline features an S/N heterocyclic five-membered ring that can be easily opened by metal ions or organic bases.[20] The formation of the benzothiazoline was demonstrated by NMR and IR spectroscopies as follows. The ^{1}H NMR spectra for **L1**−**L3** in $CDCl_3$ showed a single product isolated from each reaction. The benzothiazoline methine −C*H*− proton of **L1** and **L2** are identified at 6.41 and 6.38 ppm, respectively, which fall within the expected range of methine resonances, rather than the C*H*═N resonance (pyridine-imines ∼8.0 ppm).[18,19] The two ligands exhibit amine N*H* protons at 5.06 and 5.12 ppm, and the methyl proton of **L2** resonates at 2.55 ppm as expected for 2-methylpyridine. Although **L3** does not have a C*H* proton, its existence was indicated by N*H* resonance at 6.17 ppm. None of the ligands exhibit a thiol S*H* resonance, usually observed at ∼3 ppm.[21] The ^{13}C NMR spectra in $CDCl_3$ for the three ligands are also consistent with the benzothiazoline structures. For example, all three ligands show the hallmark features for methine carbon (CH) near

DOI: 10.1021/acs.inorgchem.8b01185
Inorg. Chem. XXXX, XXX, XXX−XXX

Scheme 5. Synthetic Pathways for Non-bulky Benzothiazoline Ligands

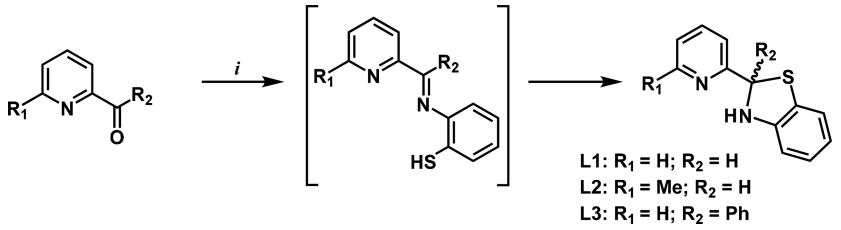

Scheme 6. Synthetic Pathways for Iron Complexes Derived from Non-bulky Benzothiazoline (A for L1; B for L2 and L3)[a]

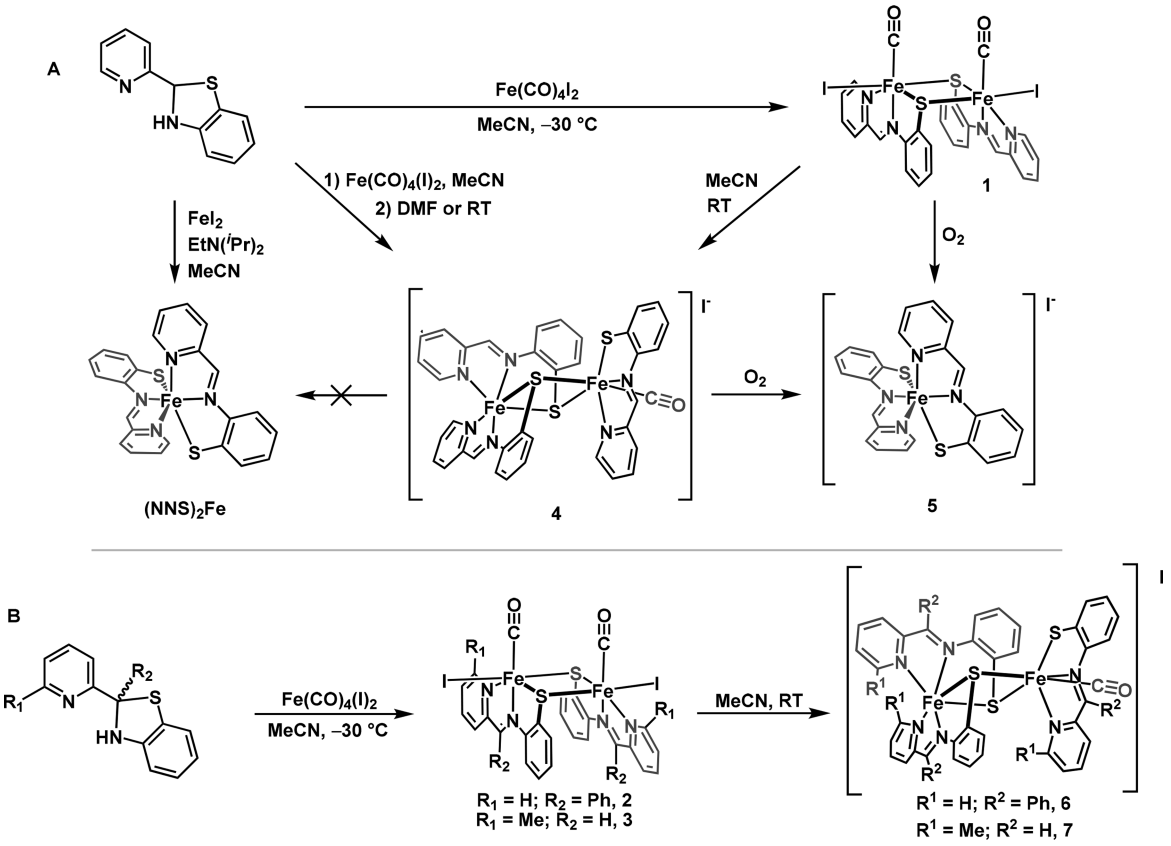

[a]See text above for discussion of **1** → **4** conversion stoichiometry.

70 ppm (70.08 ppm for **L1**, 70.26 ppm for **L2**, 82.24 ppm for **L3**).[22] It has been speculated that an equilibrium of benzothiazoline and imine may be present in the solution.[20] However, in the present study no such equilibrium was evident in the ^{1}H or ^{13}C NMR spectra. This result is consistent with the study of Tyler and co-workers, who also proposed the formation of benzothiazoline as the only product in both solid and solution.[18,19] Lastly, none of the IR spectra of the three ligands exhibit a feature typical for the ν(SH) stretch (generally ~2500 cm^{-1}).[23] All of the above characterization data support the benzothiazoline formation for **L1**, **L2**, and **L3**.

Metal Complexes of Non-bulky Ligands. The syntheses of the iron carbonyl complexes of the non-bulky ligands **L1**–**L3** are summarized in Scheme 6. The metalation of **L1**–**L3** with $[Fe(CO)_4(I)_2]$ was pursued in MeCN at −30 °C to thermally stabilize the CO ligands bound to the iron center. The bridging promiscuity of the thiolate donor promotes dimerization of the iron complexes in all three cases, yielding the dimeric dicarbonyl complexes $[(NNS)_2Fe_2(CO)_2(I)_2]$ (**1**), $[(N^{Ph}NS)_2Fe_2(CO)_2(I)_2]$ (**2**), and $[(^{Me}NNS)_2Fe_2(CO)_2(I)_2]$ (**3**). These dark green products are stable for weeks in solid state at −30 °C under inert atmosphere; when dissolved in weakly coordinating solvents such as MeCN or tetrahydrofuran (THF), these complexes are stable for days at −30 °C. At room temperature, the dimeric dicarbonyl complexes in MeCN rapidly transform to the dinuclear *mono*carbonyl complex, $[(NNS)_3Fe_2(CO)]I$ (**4**), $[(N^{Ph}NS)_3Fe_2(CO)]I$ (**6**), and $[(^{Me}NNS)_3Fe_2(CO)]I$ (**7**), as evidenced by UV/vis and X-ray diffraction (vide infra). Complex **4** can be independently synthesized first by treatment of **L1** with $[Fe(CO)_4(I)_2]$ at −30 °C, followed by crystallization with a trace amount of dimethylformamide (DMF) in MeCN. The green crystals of **4** are stable in solid state under inert atmosphere, and a MeCN solution of **4** can be stored under light at ambient temperature without loss of CO. The sharp contrast of stability between **1** and **4** indicates that the NNS ligand—specifically, inclusion of the thiolate moiety—does not generate a stable iron dicarbonyl core. Additionally,

DOI: 10.1021/acs.inorgchem.8b01185
Inorg. Chem. XXXX, XXX, XXX−XXX

Scheme 7. Synthesis of Bulky Ligand, L_B, Ultimately Derived from Isomerization of the Intended Schiff Base Ligand[a]

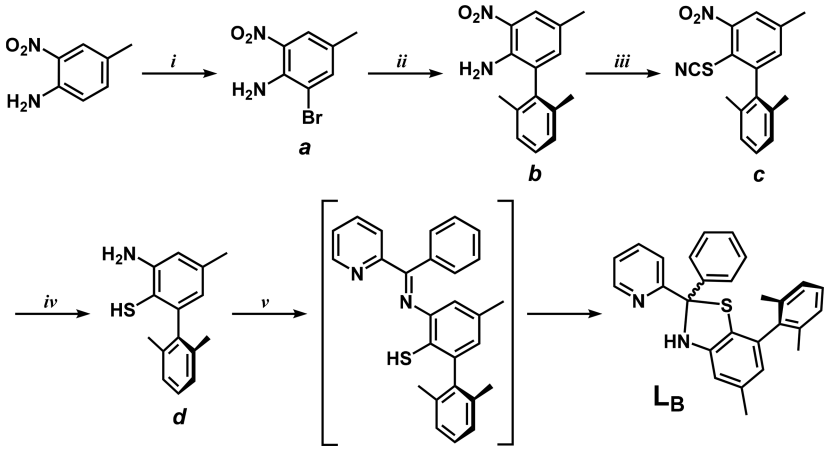

[a]Reaction conditions: (i) NH_4Br, 30 wt % H_2O_2, AcOH, rt; (ii) 2,6-dimethylphenyl boronic acid, K_2CO_3, $Pd(dba)_2$, XPhos, THF/H_2O (5:1, v/v), reflux; (iii) H_2SO_4, $NaNO_2$, H_2O/acetone, 0 °C; KSCN, CuSCN, rt; (iv) $LiAlH_4$, THF, reflux; (v) 2-benzoylpyridine, AcOH, r.t.

Scheme 8. Synthesis of the Iron Complexes 8 and 9 Derived from the Bulky Thiolate Ligand

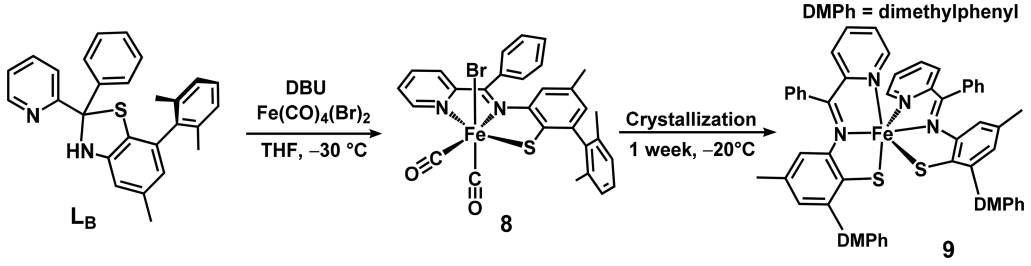

as indicated by the **1** → **4** conversion in trace DMF, strongly coordinating solvents easily replace one of the CO ligands, generating the thermodynamically more favorable monocarbonyl complexes, for example $[(NNS)_3Fe_2(CO)]I$ (**4**). In terms of the stoichiometry of the **1** → **4** conversion, complex **1** likely first loses one CO ligand. Then two-thirds of the decarbonylated intermediate obtains a third ligand, provided by the other one-third of the intermediate, thus forming complex **4**. The 1/3 equiv of Fe_2I_2 core (plus two released I^-) then forms 2 equiv of an unrecovered $Fe(I)_2(solv)$ species:

$$3L_2Fe_2I_2(CO)_2 \rightarrow 2[L_3Fe_2(CO)]I + 2FeI_2 + 4CO \quad (1)$$

On the one hand, attempts to further decarbonylate **4** to prepare the bis-ligated Fe(II) complex $[(NNS)_2Fe]$ with UV light were unsuccessful (for comparison, $[(NNS)_2Fe]$ was synthesized separately); the single CO is tightly bound to the Fe center. On the other hand, an MeCN solution of **4** is oxidized by air within seconds, turning the dark green solution to gray. Crystallization of this species afforded green crystals of the bis-ligated Fe(III) complex $[(NNS)_2Fe]I$ (**5**), whose BPh_4 salt was previously reported by Mascharak.[24] The extreme sensitivity of **4** to oxygen is also indicated by the fact that single crystals of **5** were on occasion isolated in attempts to prepare **4** in the drybox, and a minority presence of **5** is evident in the elemental analysis of **4**. As no reactivity or further measurements (other than routine characterization) were performed on **4**, the minority presence of **5** in bulk crystalline samples of **4** proved inconsequential.

Bulky Ligand and Its Metal Complex. The dimerization issue encountered above prompted us to increase the steric bulk of the thiolate to facilitate formation of a mononuclear thiolate complex. In this strategy, a bulky substituent (2,6-dimethylphenyl) was installed ortho to the thiolate donor. The synthetic pathway is represented in Scheme 7. Starting with 4-methyl-2-nitroaniline, bromination at the 6-position was performed in acetic acid using NH_4Br/H_2O_2 as a bromine source. The purpose of starting with 4-methyl-2-nitroaniline, rather than 2-nitroaniline, was to prevent the bromination at the 4-position, which otherwise decreased the yield and prevented clean separation. Subsequently, Suzuki coupling of ***a*** with 2,6-dimethylphenyl boronic acid afforded the dimethylphenyl-appended nitroaniline ***b***; the reaction proceeded with good yields only with bis(dibenzylideneacetone)palladium(0)/XPhos as catalyst. The preparation of ***c*** was performed via diazotization (acetone/H_2O, 0 °C, $NaNO_2$, H_2SO_4) followed by the addition of KSCN and CuSCN. The subsequent one-pot reduction of the nitro and thiocyanate groups was achieved with $LiAlH_4$ in dry THF, producing the expected product ***d***. Finally, condensation of ***d*** with 2-benzoylpyridine in acetic acid afforded the target ligand L_B in its "apo-form" as the benzothiazoline, as evidenced by ^1H NMR (N-*H* = 4.71 ppm) and ^{13}C NMR (methine *C*-H = 83.70 ppm).

Similar to the method described above, metalation of the bulky ligand L_B with $[Fe(CO)_4(Br)_2]/[Fe(CO)_4(I)_2]$ (Scheme 8) in THF at −30 °C was attempted. However, these conditions resulted in crude products with ν(CO) stretches exclusively above 2000 cm^{-1}; this is distinct from complexes **1**−**4**, which exhibit ν(CO) features in the 1950 cm^{-1} region. Such high-energy ν(CO) features are consistent with the ligation of a neutral thioether donor[14] (e.g., benzothiazoline), rather than the intended thiolate. We thus inferred that, for the bulky ligand, base might be necessary to promote the desired

DOI: 10.1021/acs.inorgchem.8b01185
Inorg. Chem. XXXX, XXX, XXX−XXX

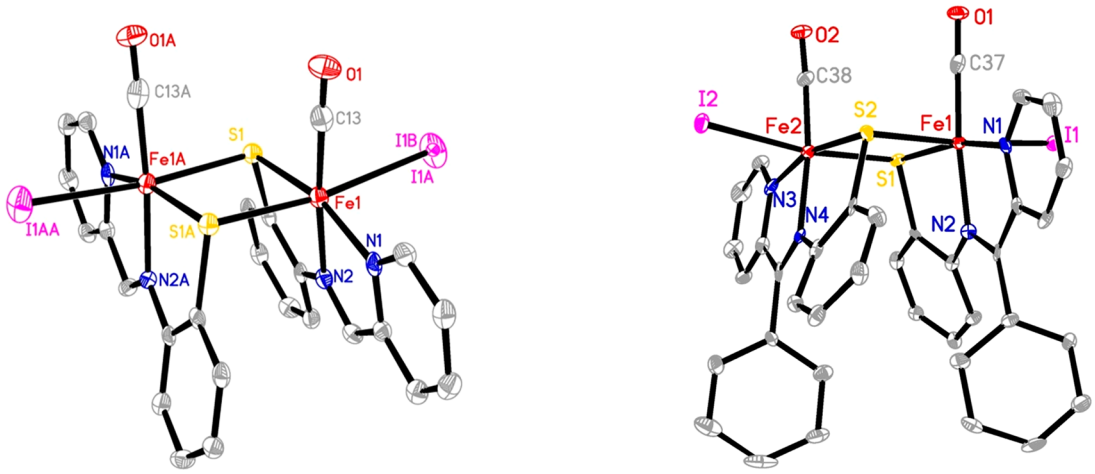

Figure 1. ORTEP diagrams (30% thermal ellipsoids) for $[(NNS)_2Fe_2(CO)_2(I)_2]$ (**1**) and $[(N^{Ph}NS)_2Fe_2(CO)_2(I)_2]$ (**2**). H atoms are omitted for clarity.

ring-opening reaction *prior to* rather than *during* metalation. We subsequently found that, when using $[Fe(CO)_4(Br)_2]$ as a metal source, anionic bases such as acetate (K^+ or NEt_4^+ salt) resulted in decarbonylation of the iron starting salt, whereas bulky and neutral nitrogen bases such as Hünig's base and proton sponge successfully promoted ring-opening and thiolate ligation, vis a vis generation of ν(CO) features (below 2000 cm^{-1}). Ultimately, it was determined that 1,8-diazabicyclo[5.4.0]undec-7-ene (DBU) provided the cleanest product, as evidenced by two ν(CO) features in the IR. This set of ν(CO) features—one above and one below 2000 cm^{-1}—is consistent with the formulation of a mononuclear dicarbonyl species ligated by an anionic ligand frame.[10,12,25,26] By comparison, iron(II) dicarbonyls ligated by neutral NNS ligands (with methylthioether donor) exhibit *both* ν(CO) stretches above 2000 cm^{-1}.[14] Thus, the product was postulated as the target complex, $[(N^{Ph}NS^{DMPh})Fe(CO)_2Br]$ (**8**); further spectroscopic evidence for **8** is provided below. Comparatively, the reactions of $[Fe(CO)_4(I)_2]$ with the bulky ligand only afforded product with ν(CO) stretches above 2000 cm^{-1}, regardless of the addition of bases. This may indicate that, in the presence of $[Fe(CO)_4(I)_2]$, the pK_a of NH is not decreased as with $[Fe(CO)_4(Br)_2]$, and stronger base may be required to convert the ligand into Schiff base; such conditions were not pursued upon obtaining the successful result with $[Fe(CO)_4(Br)_2]$.

Concerning the above observations, the use of a base in the reaction proved imperative to generate the desired bulky ring-opened Schiff base ligand. In contrast to the non-bulky ligands (no base required), the base-specificity when metalating with the bulky $\mathbf{L_B}$ is likely due to its large steric hindrance, which likely prevents the metal source from pre-emptively binding to either the N or S moiety, thus precluding a decrease in NH pK_a that would be expected upon such "pre"-complexation. The importance of choosing the proper solvent for metalation was also noticed in this reaction. THF evidently provided a suitable "middle ground" in terms of coordinating ability. The same reactions in MeCN or dichloromethane (DCM) afforded products with multiple or no ν(CO) features, respectively.

Upon crystallization in THF at −30 °C, the complex **8** gradually decomposed, affording a diamagnetic bis-ligated Fe(II) complex, $[(N^{Ph}NS^{DMPh})_2Fe]$ (**9**). The structure is shown in Figure S29, and the selected bond distances and angles are tabulated in the Supporting Information (Table S1). The *mono*carbonyl intermediate was not isolated, nor was it spectroscopically identified (vide infra).

Characterization of the Non-bulky Thiolate Complexes. *X-ray Structures.* The complex $[(NNS)_2Fe_2(CO)_2(I)_2]$ (**1**) (Figure 1) crystallized in monoclinic *C*2/*c*. The structure is a neutral dimeric complex with an $[Fe_2(S_{thiolate})_2]$ core. The two monomers are symmetric to each other with respect to a C_2 axis. Each Fe(II) ion exhibits pseudo-octahedral geometry, consisting of a NNS ligand coordinated in meridional fashion, a carbonyl, an iodide ion, and another (bridging) thiolate sulfur. The N_{py}–Fe, Fe–C(O), and C≡O distances are 1.979(5), 1.789(8), and 1.114(8) Å, respectively, which are within the normal range for a low-spin Fe(II) ion.[14,16,27] In addition, there are two unique Fe–S distances: the primary NNS thiolate bound to Fe (2.2889(17) Å) and the S-donor from the neighboring NNS ligand (2.3276(18) Å).

The structure of $[(N^{Ph}NS)_2Fe_2(CO)_2(I)_2]$ (**2**) (Figure 1) is also dimeric, and the Fe(II) centers exhibit pseudo-octahedral geometry. The coordination environment of the complex is the same as that of **1**, and the bond lengths are within the expected range for low-spin Fe(II) center (Table S1).[14,16,27] However, the phenyl ring on the Schiff base linkage slightly changes the structure of the complex, compared with **1**. The Schiff base phenyl rings are tilted away from the plane of ligand backbone, with dihedral angles of 63.52° and 67.68°. Notably, because of the steric hindrance of Schiff base phenyl rings, the planes of two ligand backbones are not parallel, and the dihedral angle between them in **2** (34.93°) is larger than that of **1** (21.29°). Another subtle difference between **2** and **1** is the "bite angle" provided by the NNS chelate. In unsubstituted **2**, the N_{py}–Fe–S bite angle of 98.5° is slightly more acute versus that for **1** (101.5°). Correspondingly, the spatial distance between the N_{py} and S donors in **2** (4.169 Å) is notably shorter than that for **1** (4.229 Å). Thus, the phenyl substituent in **2** causes a slight "pinching" effect in the ligand frame that is not evident in **1**. As a result, the Fe–N_{py} and Fe–S distances in **2** are shorter than those of **1** (Fe–N_{py}: 1.963(11) and 1.945(11) Å in **2**, vs 1.979(5) Å in **1**; Fe–S: 2.259(4) Å and 2.306(4) Å, vs 2.2889(17) Å); the Fe–N_{SB} bonds follow the opposite trend (1.994(10) in Å **2** vs 1.982(5) Å in **1**).

Complex $[(NNS)_3Fe_2(CO)]I$ (**4**) (Figure 2) crystallized in monoclinic $P2_1/c$ and is a cationic di-iron monocarbonyl complex with charge balance provided by an outer sphere iodide.

DOI: 10.1021/acs.inorgchem.8b01185
Inorg. Chem. XXXX, XXX, XXX–XXX

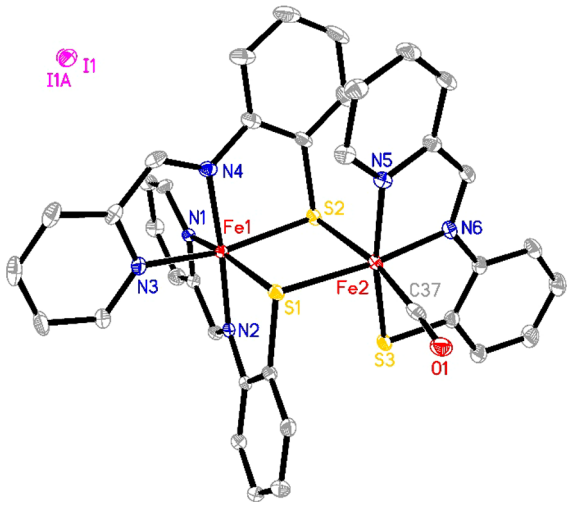

Figure 2. ORTEP diagram (30% thermal ellipsoids) for $[(NNS)_3Fe_2(CO)]I$ (**4**). H atoms are omitted for clarity.

Unlike **1**, the two Fe ions in **4** are in different coordination environments. One of the Fe ions is bis-ligated by two NNS ligands. The other Fe center is bridged by the thiolates from the bis-ligation unit, as well as coordinated by a third NNS ligand (the only non-bridging thiolate observed with L1-L3). The coordination geometry is completed by CO. Notably, **4** can be regarded as an intermediate in the transformation from **1** to **5**. The N_{py}–Fe distances are within the expected range for low-spin Fe(II) (N1–Fe1 = 1.961(3) Å, N3–Fe1 = 1.964(3) Å, N5–Fe2 = 1.988(3) Å).[14,16,27] The Fe–C(O) distance (1.774(5) Å) is slightly shorter than that of **1** but still within the normal range for low-spin Fe(II). The C≡O distance (1.115(5) Å) in **4** is comparatively longer, due to increased π back-bonding from the Fe center (compared to **1**) due to the additional ligation of the non-bridging thiolate donor.

The Fe–S bonds in **4** can be categorized into three types: $Fe1–S_{bridging}$, $Fe2–S_{bridging}$, $Fe2–S_{nonbridging}$. The $Fe2–S_{nonbridging}$ distance is the shortest [2.2733(10) Å], followed by $Fe1–S_{bridging}$ [2.2888(11) and 2.2972(10) Å], and finally the longest, $Fe2–S_{bridging}$ [2.3061(10) and 2.4026(11) Å].

Complex $[(NNS)_2Fe]I$ (**5**) (Figure 3) was crystallized in $P2_1/n$ and consists of two NNS units ligated to a single Fe(III) ion in pseudo-octahedral geometry; an outer sphere iodide provides charge balance, and a molecule of I_2 was also present as solvate. The $Fe–N_{py}$ distances are 2.015(8) and 2.016(8) Å, and the Fe–S distances are 2.212(3) and 2.222(3) Å, which are comparable with the analogous structure of $[(NNS)_2Fe]BPh_4$ obtained by Mascharak and co-workers,[24] with $Fe–N_{py}$ = 2.015, 1.977 Å and Fe–S = 2.223, 2.211 Å. For comparison, the Fe(II) bis-ligated complex $[(NNS)_2Fe]$ was synthesized and crystallized independently in $Pna2_1$. The $Fe–N_{py}$ distances are shorter than those of **5** (1.973(9) and 1.961(10) Å), and Fe–S distances are longer than those of **5** (2.290(3) and 2.294(3) Å). The changes in bond distances are likely due to the higher oxidation state, which facilitates the bonding between anionic-S donor with the cationic Fe(III).

IR Spectroscopy. The solid-state IR spectra of the non-bulky thiolate complexes were recorded under N_2 atmosphere and are shown in the Supporting Information (Figures S16–S20); the values are tabulated in Table 1. The CO peaks for **1**, **2**, and **3** are observed below 2000 cm^{-1}, which correspond to the symmetric (higher wavenumber) and asymmetric stretches of the two CO ligands. The similar wavenumbers of CO peaks in **1**, **2**, and **3** show negligible change of the electron density at the metal center, whereas modification of the ligand backbone (i.e., adding methyl group on the ortho position of pyridine or phenyl group on the imine carbon) decreases the intensity of the asymmetric stretching of CO (1932 cm^{-1} for **2** and 1927 cm^{-1} for **3**). Small $\Delta\nu$ (<50 cm^{-1}) and different intensity between symmetric and asymmetric CO stretches suggest that the CO ligands do not bind to Fe center in a cis orientation.[26] These values are in line with the density functional theory (DFT)-calculated IR frequency (2028 cm^{-1} for symmetric vibration; 2005 cm^{-1} for asymmetric vibration). For **4**, a single CO vibration is observed at 1940 cm^{-1}, which is consistent with the X-ray structure of **4** as a monocarbonyl complex.

Table 1. Selected ν(CO) IR Features for the Non-bulky and Bulky Thiolate Complexes

cmpd	1	2	3	4
experimental	1941, 1926	1955, 1932	1951, 1927	1940
calculated	2028, 2005			2023

Experimental and DFT Characterization of the Bulky Thiolate Monomer 8. Although the instability of the complex **8** prevented its crystallization, the formation of the mononuclear dicarbonyl complex $[(N^{Ph}NS^{DMPh})Fe(CO)_2Br]$ (**8**) was evidenced by spectroscopic data (IR and ^{13}C NMR) and DFT calculation. The IR spectrum (Figure 4) of **8** shows two

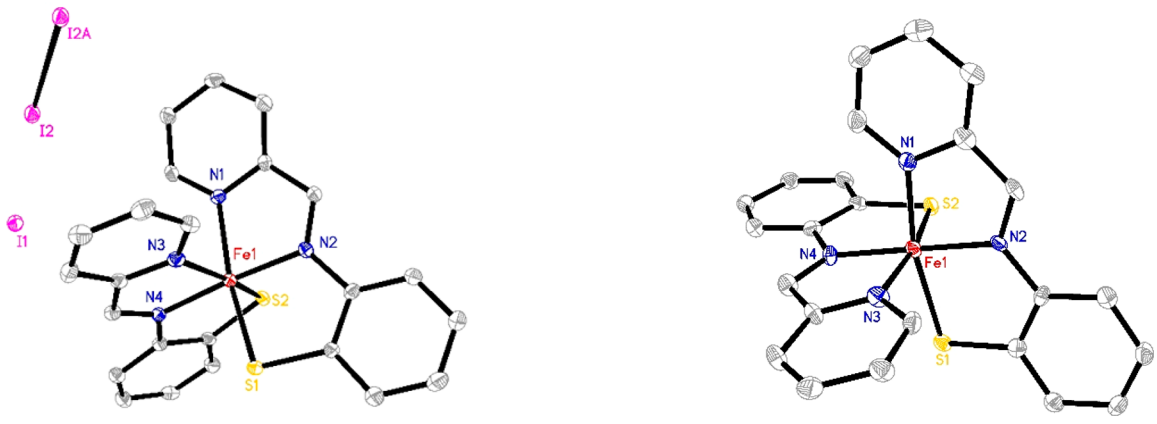

Figure 3. ORTEP diagrams (30% thermal ellipsoids) for $[(NNS)_2Fe]I{\cdot}I_2$ (**5**·I_2) and $[(NNS)_2Fe]$. H atoms are omitted for clarity.

DOI: 10.1021/acs.inorgchem.8b01185
Inorg. Chem. XXXX, XXX, XXX–XXX

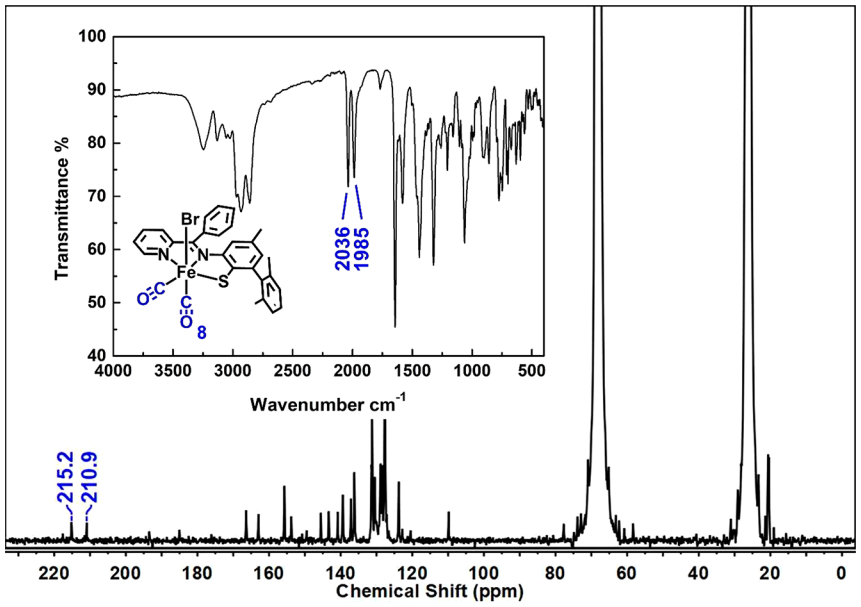

Figure 4. Low-temperature (−30 °C) ^{13}C NMR spectrum of **8** (solvent: THF. The complex was generated in situ at −30 °C under CO atmosphere). (inset) Solid-state IR spectrum of **8**.

carbonyl peaks at 2036 and 1985 cm^{-1}, which are blue-shifted ∼90 cm^{-1} compared with those of the dimer complexes (**1**, **2**, and **3**). The equal intensity and $\Delta\nu$ of the two CO frequencies is ∼51 cm^{-1}, larger than those of the dimers. Both of the above features suggest that the two COs are bound to one iron center in a cis fashion.[26] Compared with the CO stretch of FeGP cofactor (solid:[28] 2004 and 1934 cm^{-1}; solution:[26] 2031 and 1972 cm^{-1}), the CO frequencies are blue-shifted, indicating that the electron density of the Fe center in the NNS complex is less than that in the enzyme active site.

The ^{13}C NMR spectrum of **8** was obtained at −30 °C with the in situ prepared complex in THF. The NMR tube was charged with CO gas (1 atm) to prevent decomposition. The ^{13}C NMR exhibits two resonances in the far downfield region at 215.2 and 211.9 ppm, which are assigned as the two chemically inequivalent COs. The chemical shifts of the COs are comparable with other reported complexes with *cis*-$\{Fe(CO)_2\}^{2+}$ motif (195−220 ppm).[12,29] The possibility of the presence of **8** as a dinuclear dicaronyl complex can be excluded, as in those cases the two terminal COs are chemically equivalent and would only display a single resonance in the ^{13}C NMR spectrum.

Attempts of observing **8** in mass spectrometry were unsuccessful, as the dicarbonyl complex decomposed during electrospray ionization (ESI) or chemical ionization (CI) process. Instead, the ESI-MS analysis shows two peaks with m/z = 463.0944 and 565.0036, consistent with the formulations of monomeric $[(N^{Ph}NS^{DMPh})Fe]^+$ and $[(N^{Ph}NS^{DMPh})FeBr+Na]^+$, respectively.

To further postulate the formation of the mononuclear iron(II) dicarbonyl complex **8**, DFT calculations were performed at the level of B3LYP/6-311G** for C, H, O, N, S, Br and B3LYP/SDD for Fe. Geometry optimization provided a converged mononuclear diamagnetic Fe(II) structure featuring cis terminal carbonyls (Figure 5). The selected bond lengths and angles are shown in the Supporting Information (Table S1). The calculated IR of **8** (Figure 5) also exhibits two CO stretching features at 2044 and 2020 cm^{-1}, corresponding to the symmetric and asymmetric vibrations, respectively. Notably, the

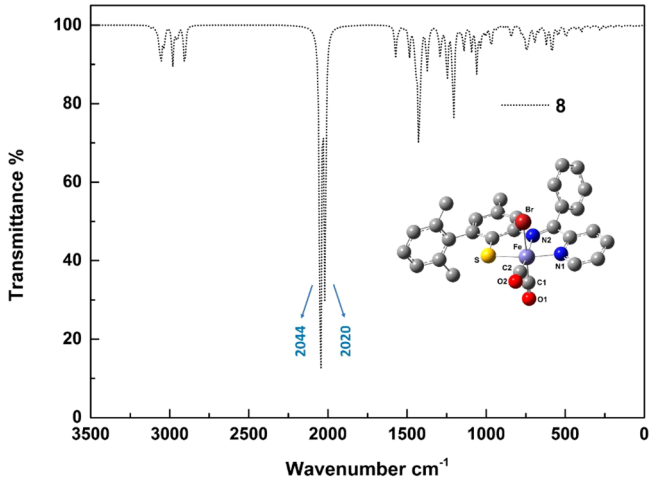

Figure 5. DFT-calculated structure and IR spectrum of **8**.

two CO vibrations are almost equally intense, which is in contrast to the calculated CO intensities for $[(NNS)_2Fe_2(CO)_2I_2]$ (**1**), where the CO symmetric vibrations are significantly more intense than the asymmetric vibration (Figures S31 and S32). In addition, the wavenumber of CO vibrations for **8** is blue-shifted by 20 cm^{-1}, compared to the calculated value of **1**. The same trend is evident in the experimental data.

On the basis of the above data, the increase of the steric hindrance of the NNS ligand considerably affects the product afforded from the metalation. The bulky aryl substituent 2,6-dimethylphenyl (DMPh) facilitates the formation of the mononuclear *cis*-dicarbonyl complex **8**.

Thermal Stability of the Dicarbonyl Complexes. We demonstrated the different ligation properties of the non-bulky and bulky NNS ligands. The thermal instability of the dicarbonyl complexes (**1**, **2**, **3**, and **8**) are also observed qualitatively in the synthesis. To quantitatively compare the ability of the NNS ligands to stabilize the carbonyl complexes, time-dependent UV/vis and IR experiments were performed.

DOI: 10.1021/acs.inorgchem.8b01185
Inorg. Chem. XXXX, XXX, XXX−XXX

The dimeric dicarbonyl complexes **1**−**3** were synthesized in situ in MeCN at low temperature (−30 °C) with a concentration of ∼0.5 mM. The solutions were quickly transferred to an air-free cuvette, and the changes in UV/vis absorption spectra were monitored at room temperature in the dark (Figure S38). All the samples gradually converted to the corresponding monocarbonyl complexes; the conversions are plotted in Figure 6.

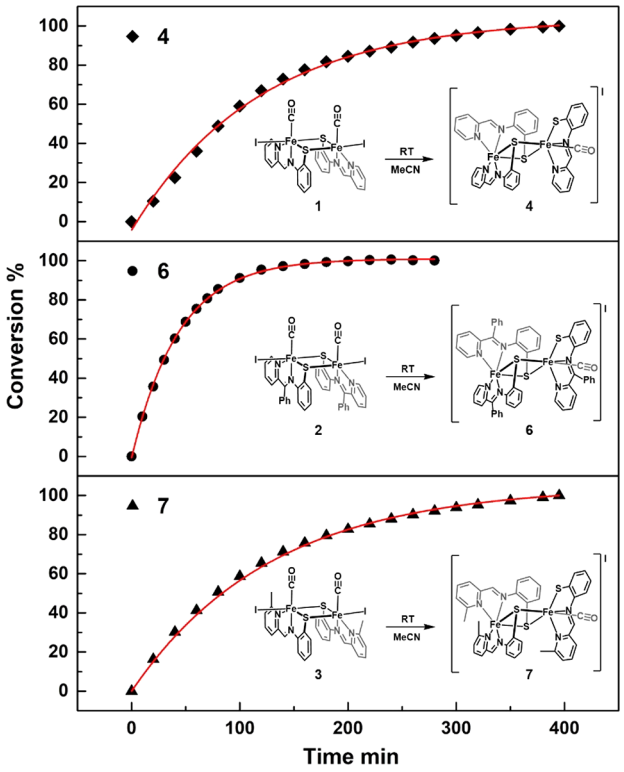

Figure 6. Conversion of **1**, **2**, and **3** to the corresponding Fe(II) monocarbonyls **4**, **6**, and **7**, respectively, as determined by changes in the UV/vis spectra (changes of absorbance were monitored at the wavelength of 731 nm for **1**, 766 nm for **2**, and 430 nm for **3**).

The variation of the ligand backbone gave rise to different $t_{1/2}$ values. Complex **2** shows the shortest $t_{1/2}$ (30 min), whereas complexes **3** and **1** exhibit similar stabilities ($t_{1/2}$: 75 min for **3**, 80 min for **1**). The difference in $t_{1/2}$ can be attributed to the structural distortion eident in the crystal structures. As the structure of **2** shows, the phenyl moiety on the imine carbon prevents ligand backbone from attaining ideal planarity in the crystal (see X-ray section), which decreases the stability of **2**. In contrast, in **3** the methyl group at the ortho position of pyridine does not twist the ligand backbone, thus rendering a similar $t_{1/2}$ as **1**. In contrast, the monocarbonyl complexes (**4**, **6**, and **7**) are quite stable at room temperature in the inert atmosphere; no change in the UV/vis spectra was observed at room temperature over the course of several days.

Attempts to monitor the decomposition of the mononuclear dicarbonyl complex $[(N^{Ph}NS^{DMPh})Fe(CO)_2Br]$ (**8**) by UV/vis proved unsuccessful, as **8** is unstable at room temperature, and the absorption spectrum of the bis-ligated complex **9** completely obscures the trace of **8** (Figure S39). Thus, we instead monitored the solution IR of **8** to study its thermal stability. A THF solution of **8** was incubated in the dark at room temperature, and an IR spectrum was acquired every minute. As shown in Figure 7, the thermal stability of **8** is

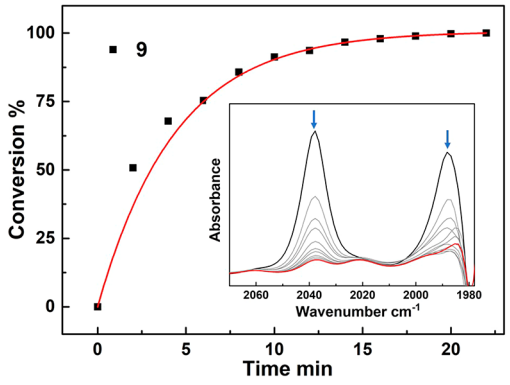

Figure 7. Conversion of **8** to the bis-ligated Fe^{II} complex **9** as determined by changes in the solution IR spectra in THF (inset).

considerably shorter than those dimeric dicarbonyl complexes. The conversion of **8** to **9** is complete within 15 min, with $t_{1/2}$ = 2 min. During the conversion, complex **8** loses two CO ligands simultaneously, and the dimeric dicarbonyl complex was not observed (Figure 7 inset).

Overall, it is evident that the NNS(thiolate) ligand frame is unable to stabilize the *cis*-dicarbonyl motif—regardless of mono- or dinuclearity—leading to decarbonylation and the (half)bis-ligated complexes. This suggests that one of the critical roles of the organometallic Fe−C(acyl) moiety in the Hmd enzyme active site is to prevent thermalization of the CO ligands under biological temperature and conditions. An analogous effect is also observed in our previous research,[14,16] whereas the incorporation of carbamoyl unit to the Fe center resulted in a series of stable organometallic complexes of type $[(O{=}C^{NH}N^{py}S^{Me})Fe(CO)_2L]$.[15,16]

CONCLUSIONS

(1) This series of iron carbonyl complexes featuring Schiff-base pyridine/(NNS) thiolate have been prepared via one-step metalation using benzothiazoline ligand precursors and iron tetracarbonyl halides.

(2) Upon metalation, the non-bulky NNS thiolate ligands produce diiron dicarbonyl complexes due to the thiolate bridging effect. The products of stepwise decarbonylation of diiron dicarbonyl complexes are diiron monocarbonyl complexes; finally, the oxidized iron(III) bis-ligated complexes were isolated.

(3) A bulky thiolate ligand with a 2,6-dimethylphenyl group ortho to the (aryl)thiolate was developed. This functional group prevents the dimerization across the thiolate, thereby affording a mononuclear dicarbonyl complex. This strategy could be applied to the synthesis of future structural and functional model of [Fe]-hydrogenase.

(4) The stability study has shown that the thiolate (without the acyl unit) is not sufficient to stabilize the *cis*-$\{Fe(CO)_2\}^{2+}$ core and that ensuing decarbonylation leads to the formation of a bis-ligated complex. This indicates that one of functions of the acyl unit in the active site of [Fe]-hydrogenase is to prevent thermalization of the CO ligands bound to the Fe center.

EXPERIMENTAL SECTION

General Procedures and Reagents. All organic starting materials were purchased from Acros Organics or Sigma-Aldrich and used without further purification. The Fe(II) starting salt $[Fe(CO)_4(I)_2]$ was prepared by reaction of $[Fe(CO)_5]$ (Strem) with I_2 according to

DOI: 10.1021/acs.inorgchem.8b01185
Inorg. Chem. XXXX, XXX, XXX−XXX

the published procedure.[30] The Fe(II) starting salt $[Fe(CO)_4(Br)_2]$ was prepared by reaction of $[Fe(CO)_5]$ (Strem) with Br_2, according to the published procedure,[25] but purified by recrystallization from CH_2Cl_2 at −20 °C instead of sublimation. All iron complexes were prepared inside the glovebox under dinitrogen atmosphere in the dark, unless otherwise indicated. High-performance liquid chromatography (HPLC)-grade solvents were purchased from EMD, Fisher, Macron, or J.T. Baker and dried through an alumina column system (Pure Process Technology). Deuterated solvent ($CDCl_3$) was purchased from Cambridge Isotopes and used as received.

Ligand Syntheses. *NNS 2-(Pyridin-2′-yl)benzothiazoline (**L1**).* The synthesis of **L1** was a modified version of a published procedure.[31] Under dinitrogen atmosphere, 2-pyridinecarboxaldehyde (1.000 g, 9.337 mmol) was mixed with 2-aminobenzenethiol (1.167 g, 9.337 mmol), upon the addition of which a pale yellow precipitate formed immediately. Then, 2 mL of methanol was added, and the reaction was stirred for 10 min. The methanol was decanted, and the residue was washed with pentane. The product was collected as a pale yellow solid. Yield: 1.930 g (96.5%). IR (neat, cm^{-1}) 3185 m, 3166 m, 3067 w, 3015 w, 2953 w, 1589 m, 1577 m, 1467 s, 1434 m, 1421m, 1348 m, 1306 m, 1268 w, 1250 m, 1158 m, 1146 m, 1120 m, 1098 m, 1071 m, 1048 m, 1017 m, 996 w, 957 w, 911 m, 905 w, 794 m, 768 m, 745 s, 733 s, 716 s, 685 s, 646 m, 620 s, 572 w, 562 w, 529 m,478 s; ^1H NMR (400 MHz, $CDCl_3$) δ = 8.56 (ddd, J = 4.9, 1.8, 1.0 Hz, 1H), 7.69 (ddd, J = 7.4, 1.8, 0.4 Hz, 1H), 7.58 (dtd, J = 7.9, 1.1, 0.5 Hz, 1H), 7.22 (dddd, J = 7.5, 4.8, 1.2, 0.4 Hz, 1H), 7.12−7.02 (m, 1H), 7.01−6.91 (m, 1H), 6.86−6.75 (m, 2H), 6.41 (s, 1H), 5.06 (s, 1H); ^{13}C NMR (100 MHz, $CDCl_3$) δ = 160.4, 149.2, 146.7, 137.4, 127.7, 125.6, 123.3, 121.9, 121.6, 121.1, 111.7, 70.1; MS (ESI, m/z): 215 $[MH]^+$, 237 $[MNa]^+$.

*^{Me}NNS 2-(6′-Methyl-pyridin-2′-yl)benzothiazoline (**L2**).* Under dinitrogen atmosphere, 6-methyl-2-pyridinecarboxaldehyde (0.985 mg, 8.131 mmol) was mixed with 2-aminobenzenethiol (1.017 g, 8.131 mmol), upon the addition of which a pale yellow precipitate formed immediately. Then, 1 mL of methanol was added, and the reaction was stirred for 10 min. The methanol was removed in vacuo. The resulting orange oil was triturated with Et_2O/pentane (v/v = 1/4, 5 mL) and washed with pentane (3 mL), which afforded the product as a pale yellow solid. Yield: 1.429 g (76%). IR (neat, cm^{-1}) 3136 br, 3066 m, 3007 w, 2935 w, 2884 m, 1591 s, 1571 s, 1498 w, 1446 s, 1374 w, 1305 w, 1275 w, 1251 w, 1149 m, 1114 w, 1085 m 1056 m, 1032 w, 1018 m, 989 m, 808 m, 731 s, 690 m, 421 w; ^1H NMR (400 MHz, $CDCl_3$) δ = 7.58 (t, J = 7.7 Hz, 1H), 7.37 (d, J = 7.7 Hz, 1H), 7.11−7.05 (m, 2H), 6.99−6.93 (m, 1H), 6.80 (d, J = 7.8 Hz, 2H), 6.38 (s, 1H), 5.12 (s, 1H), 2.55 (s, 3H); ^{13}C NMR (100 MHz, $CDCl_3$) δ = 159.4, 158.04, 146.9, 137.5, 128.2, 125.5, 122.9, 121.8, 121.6, 118.1, 111.9, 70.3, 24.5; MS (ESI, m/z): 229 $[MH]^+$, 251 $[MNa]^+$.

*N^{Ph}NS 2-(Pyridin-2′-yl)-2-phenyl-benzothiazoline (**L3**).* Under dinitrogen atmosphere, 2-benzoylpyridine (1.000 g, 5.460 mmol) was mixed with 2-aminobenzenethiol (0.750 g, 6.000 mmol), and 10 mL of acetic acid was added. The reaction was stirred at *room temperature* for 24 h. The acetic acid was removed in vacuo. The resulting oil was triturated with ethanol (3 × 3 mL), Et_2O (3 mL), and pentane (3 mL), which afforded the product as a pale yellow solid. Yield: 1.130 g (71%). IR (neat, cm^{-1}) 3258 m, 3058 w, 2979 m, 2875 w, 1607 w, 1582 m, 1474 w, 1458 m, 1446 m, 1275 m, 1212 w, 1119 w, 1032 w, 904 w, 763 s, 749 s, 730 m, 714 m, 576 w, 454 w; ^1H NMR (400 MHz, $CDCl_3$) δ = 8.67−8.51 (m, 1H), 7.84 (d, J = 7.9 Hz, 1H), 7.69 (td, J = 7.7, 1.8 Hz, 1H), 7.65−7.50 (m, 2H), 7.47−7.27 (m, 2H), 7.25 (d, J = 7.3 Hz, 1H), 7.22−7.12 (m, 1H), 7.06 (dd, J = 7.6, 1.3 Hz, 1H), 6.95 (td, J = 7.6, 1.3 Hz, 1H), 6.83 (dd, J = 7.9, 1.2 Hz, 1H), 6.77 (td, J = 7.5, 1.2 Hz, 1H), 6.17 (s, 1H); ^{13}C NMR (100 MHz, $CDCl_3$) δ = 163.0, 148.8, 146.1, 144.5, 136.8, 128.3, 127.8, 127.1, 125.6, 122.5, 121.8, 121.3, 121.2, 111.8, 84.2; MS (ESI, m/z): 291 $[MH]^+$, 313 $[MNa]^+$.

2-Bromo-4-methyl-6-nitrobenzenamine (a). 4-Methyl-2-nitroaniline (5.00 g, 32.90 mmol) was dissolved in acetic acid (50 mL). Finely ground ammonium bromide (5.16 g, 52.60 mmol) and 30 wt % solution of hydrogen peroxide (in H_2O) (5.25 mL, 52.60 mmol) were added consecutively to reaction mixture, which then was stirred for 68 h. The mixture was poured into an aqueous solution of 1 M sodium carbonate, and the precipitate was collected by filtration and dried in vacuo to afford **a** as a pure, bright orange powder. Yield: 7.13 g (93.8%). IR (neat, cm^{-1}) 3481 m, 3466 m, 3367 s, 3355 s, 1621 m, 1573 s, 1551 s, 1504 s, 1445 m, 1395 m, 1344 s, 1323 s, 1251 s, 1237 s, 1201 s, 1086 s, 935 s, 865 s, 791 m, 761 s, 727 s, 551 s, 458 m; ^1H NMR (400 MHz, $CDCl_3$) δ = 7.93 (s, 1H), 7.55 (d, J = 2.0 Hz,1H), 6.46 (s, 2H), 2.27 (s, 3H);^{13}C NMR (100 MHz, $CDCl_3$) δ = 140.3, 140.1, 132.7, 126.6, 125.6, 112.0, 20.0; MS (ESI, m/z): 231 $[MH]^+$.

2-(2′,6′-Dimethylphenyl)-4-methyl-6-nitroaniline (b). Under dinitrogen atmosphere, **a** (5.00 g, 21.64 mmol), 2,6-dimethylphenyl boronic acid (4.00 g, 26.67 mmol), potassium carbonate (4.00 g, 28.94 mmol), 2-dicyclohexylphosphino-2′,4′,6′-triisopropylbiphenyl (Xphos) (309 mg, 0.649 mmol), and $Pd(dba)_2$ (373 mg, 0.649 mmol) were mixed in 120 mL of degassed THF and 24 mL of degassed water. The reaction was refluxed for 24 h, after which an additional amount of 2,6-dimethylphenyl boronic acid (2.00 g, 13.34 mmol) and potassium carbonate (2.00 g, 14.47 mmol) were added and refluxed for another 24 h. After it cooled to room temperature, THF was removed in vacuo, and the mixture was extracted with ethyl acetate (50 mL × 3). The combined organic phase was washed with brine and dried over Na_2SO_4. The product was purified by column chromatography (silica gel, EtOAc/hexane = 1:8) to afford **b** as an orange oil. Yield: 4.33 g (78%). IR (neat, cm^{-1}): 1716 m, 1629 m, 1567 s, 1517 m, 1442 m, 1253 m, 1230 s, 1083 w, 1031 w, 935 m, 872 m, 768 s, 709 m; ^1H NMR (400 MHz, $CDCl_3$): δ 7.97 (d, J = 1.2 Hz, 1H), 7.25−7.21 (m, 1H), 7.17 (d, J = 7.3 Hz, 2H), 7.02 (d, J = 2.1 Hz, 1H), 5.81 (s, 2H), 2.30 (s, 3H), 2.04 (s, 6H); ^{13}C NMR (100 MHz, $CDCl_3$): δ = 140.3, 137.5, 137.3, 135.1, 132.2, 129.7, 128.5, 128.1, 126.0, 124.5, 20.2, 20.0; MS (ESI, m/z): 257 $[MH]^+$, 279 $[MNa]^+$.

2-(2′,6′-Dimethylphenyl)-4-methyl-6-nitrobenzenethiocyanate (c). To a solution of **b** (4.33 g, 16.89 mmol) in 300 mL of acetone was added 10.7 mL of sulfuric acid (202.59 mmol). $NaNO_2$ (5.82 g, 84.47 mmol) in 150 mL of water was added dropwise to the mixture at 0 °C. The reaction was stirred at 0 °C for 30 min. Then, copper thiocyante (5.34 g, 43.92 mmol) and potassium thiocyanate (16.42 g, 168.9 mmol) in 150 mL of water were added to the reaction at 0 °C. The reaction was stirred at 0 °C for 1 h and at room temperature, for 4 h. A 10 M NaOH aqueous solution was added dropwise to adjust the pH to ∼7, and acetone was removed under reduced pressure. The mixture was filtered, and the filtrate was extracted with ethyl acetate (20 mL × 3). The combined organic phase was washed with brine and dried over Na_2SO_4. The product was purified with column chromatography (silica gel, EtOAc/hexane = 1:8) to afford **c** as an orange solid. Yield: 1.92 g (38%). IR (neat, cm^{-1}): 2170 m (SCN), 1531 s, 1463 s, 1379 m, 1355 s, 1081 w, 770 s, 710 m; ^1H NMR (400 MHz, $CDCl_3$): δ 7.82 (s, 1H), 7.35 (m, 1H), 7.30 (m, 1H), 7.19 (d, J = 7.9 Hz, 2H), 2.53 (s 3H), 2.04 (s 6H); ^{13}C NMR (101 MHz, $CDCl_3$): δ = 152.5, 147.5, 143.3, 137.1, 136.5, 136.0, 129.2, 128.3, 125.4, 114.9, 108.1, 21.3, 20.8; MS (CI, m/z): 272 $[M^+$ without CN].

2-Mercapto-3-(2′,6′-dimethylphenyl)-5-methyl-aniline (d). Under dinitrogen atmosphere, **c** (500 mg, 1.676 mmol) in 15 mL of dry THF was added to $LiAlH_4$ (508 mg, 13.407 mmol) slowly at 0 °C and then refluxed for 16 h. After it was cooled to 0 °C, the reaction was quenched with degassed water and filtered under dinitrogen. The residue was washed with degassed THF (5 mL) and water (2 × 5 mL). A 1 M HCl aqueous solution was added to the filtrate until the pH was ∼3. The THF was removed in vacuo, and the compound **d** precipitated as a yellow solid, which was washed with water (3 × 10 mL) and pentane (3 × 5 mL), and used for the next step without further purification. Yield: 257 mg (63%). IR (neat, cm^{-1}): 3383 w, 3309 w, 2961 w, 2584 w (S−H), 2558 w (S−H), 1620 s, 1566 s, 1453 s, 1408 m, 1375 m, 1329 m, 1259 s, 1084 s, 1027 s, 798 m, 768 m, 567 w; ^1H NMR (400 MHz, $CDCl_3$): δ = 7.18 (dd, J = 8.6, 6.5 Hz, 1H), 7.13−7.08 (m, 2H), 6.58 (dd, J = 1.8, 0.7 Hz, 1H), 6.39 (dd, J = 1.8, 0.7 Hz, 1H), 4.02 (s, 2H), 2.61 (s, 1H), 2.26 (s, 3H), 2.00 (s, 6H); MS (CI, m/z): 244 $[MH]^+$.

$N^{Ph}NS^{DMPh}$ 2-(Pyridin-2′-yl)-2-phenyl-4-(2″,6″-dimethylphenyl)-6-methylbenzothiazoline (L_B). Under dinitrogen atmosphere,

DOI: 10.1021/acs.inorgchem.8b01185
Inorg. Chem. XXXX, XXX, XXX−XXX

d (257 mg, 1.056 mmol) and 2-benzoylpyridine (174 mg, 0.950 mmol) were mixed in 5 mL of acetic acid. The reaction was stirred at room temperature for 24 h, and a large amount of off-white precipitate was observed. The acetic acid was removed in vacuo. The oil that resulted was treated with pentane (30 mL), which afforded the product as an off-white solid. Yield: 233 mg (54%). IR (neat, cm^{-1}): 1577 m, 1464 m, 1435 m, 1409 m, 1287 w, 1210 w, 995 w, 839 m, 760 s, 701 s, 595 m, 551 m; ^1H NMR (400 MHz, $CDCl_3$, 25 °C): δ = 8.53 (d, J = 4.6 Hz, 1H), 7.80 (d, J = 8.0 Hz, 1H), 7.65 (td, J = 7.6, 1.6 Hz, 1H), 7.50 (dd, J = 8.2, 1.0 Hz, 2H), 7.26 (s, J = 15.0 Hz, 1H), 7.20 (d, J = 7.0 Hz, 1H), 7.18−7.11 (m, 2H), 7.07 (d, J = 7.7 Hz, 2H), 6.64 (s, 1H), 6.36 (s, 1H), 6.29 (s, 1H), 4.71 (s, 1H), 2.26 (s, 3H), 2.04 (s, 3H), 1.97 (s, 3H);^{13}C NMR (101 MHz, $CDCl_3$, 25 °C): δ = 163.3, 148.7, 146.5, 144.6, 140.0, 136.6, 136.2, 136.0, 135.8, 134.3, 128.2, 127.5, 127.4, 127.3, 127.2, 126.7, 123.5, 122.3, 122.0, 121.7, 111.0, 83.7, 21.3, 20.2, 20.2. MS (ESI, m/z): 409 $[MH]^+$, 431 $[MNa]^+$.

Complex Syntheses. *[(NNS)$_2$Fe$_2$(CO)$_2$(I)$_2$] (1).* Under dinitrogen atmosphere, 0.099 g (0.234 mmol) of $[Fe(CO)_4(I)_2]$ in a vial was dissolved in 4 mL of acetonitrile as a dark red solution. In a separate vial, 0.050 g (0.234 mmol) of **L1** was dissolved in another 4 mL of acetonitrile to generate a yellow solution. At −30 °C, the addition of the $[Fe(CO)_4(I)_2]$/acetonitrile solution to the ligand solution immediately generated a dark green solution, which was stirred at −30 °C for 4 h. The resulting solution was filtered, and the filtrate was subjected to vapor diffusion of diethyl ether at −30 °C, which resulted in small dark brown crystals suitable for X-ray diffraction. Yield: 52 mg (53%). IR (neat, cm^{-1}): 1941 s, 1926 s, 1601 m, 1469 m, 1456 m, 1432 m, 1149 m, 777 s, 757 s, 743 s, 580 s. UV/vis in MeCN, λ_{max} (in nm): 465, 309, 245.

[(N^{Ph}NS)$_2$Fe$_2$(CO)$_2$(I)$_2$] (2). This complex was prepared according to the procedure for $[(\mathbf{NNS})_2\mathbf{Fe}_2(\mathbf{CO})_2(\mathbf{I})_2]$ (**1**): **L3** (0.050 g, 0.172 mmol) in 4 mL of acetonitrile and $[Fe(CO)_4(I)_2]$ (0.073 g, 0.172 mmol) in 4 mL of acetonitrile. The dark brown crystals suitable for X-ray diffraction were obtained from acetonitrile solution subjected to diethyl ether vapor diffusion at −30 °C. Yield: 17 mg (21%). IR (neat, cm^{-1}): 1955 s, 1932 m, 1588 m, 1573 s, 1458 m, 1442 m, 1327 m, 1017 w, 745 s, 714 s, 617 s, 580 s, 568 s, 440 m. UV/vis in MeCN, λ_{max} (in nm) = 465, 309, 245.

[(MeNNS)$_2$Fe$_2$(CO)$_2$(I)$_2$] (3). This complex was prepared according to the procedure for $[(\mathbf{NNS})_2\mathbf{Fe}_2(\mathbf{CO})_2(\mathbf{I})_2]$ (**1**): **L2** (0.050 g, 0.219 mmol) in 4 mL of acetonitrile and $[Fe(CO)_4(I)_2]$ (0.092 g, 0.219 mmol) in 4 mL of acetonitrile. The resulting acetonitrile solution was subjected to diethyl ether vapor diffusion at −30 °C, which afforded black powder. Yield: 36 mg (38%). IR (neat, cm^{-1}): 1951 s, 1927 m, 1605 m, 1471 s, 1375 m, 1329 m, 1098 m, 794 m, 766 s, 736 s, 567 s, 424 m. UV/vis in MeCN: λ_{max} (in nm): 465, 309, 245.

[(NNS)$_3$Fe$_2$(CO)]I (4). Method A. This complex was prepared according to the procedure for $[(\mathbf{NNS})_2\mathbf{Fe}_2(\mathbf{CO})_2(\mathbf{I})_2]$, except that after the reaction, the filtrate was subjected to vapor diffusion of diethyl ether at ambient glovebox temperature, which resulted in small dark green crystals suitable for X-ray diffraction. Yield: 48 mg (69%). IR (neat, cm^{-1}): 1940 s, 1661 s, 1651 s, 1596 m, 1504 m, 1467 m, 1434 m, 1384 m, 1297m, 1287 m, 1151 s, 764 m, 712 m, 572 m. UV/vis in MeCN, λ_{max} (in nm) (ε in M^{-1} cm^{-1}): 727 (4360), 627 (3790), 424 (8470), 317 (25 500), 244 (42 000). Note: Elemental analysis for bulk crystalline material of **4** indicated the presence of **5** (~25%), which immediately forms from solutions of **4** exposed to oxygen. Although samples of **4** were synthesized and crystallized in a drybox, we attribute the presence of **5** (estimated ~25%) to two factors: first, residual O_2 in the drybox, and second, with the identical charge (monocation) and counterion (I^-) of the two complexes. Anal. calcd for $C_{37}H_{27}Fe_2N_6OS_3I$ (**4**, 75%) plus $C_{24}H_{18}FeIN_4S_2$ (**5**, 25%): C 48.75, H 3.00, N 9.25%; found: C 46.50, H 3.73, N 9.76%.

Method B. The $[(\mathbf{NNS})_3\mathbf{Fe}_2(\mathbf{CO})]\mathbf{I}$ was prepared according to the procedure for $[(\mathbf{NNS})_2\mathbf{Fe}_2(\mathbf{CO})_2(\mathbf{I})_2]$, except that, after the reaction, the filtrate was treated with several drops of DMF and subjected to vapor diffusion of diethyl ether at −30 °C, which resulted in small dark green crystals suitable for X-ray diffraction.

[(NNS)$_2$FeI·0.25I$_2$ (5). This complex was prepared according to the procedure for $[(\mathbf{NNS})_3\mathbf{Fe}_2(\mathbf{CO})]\mathbf{I}$, except that after the reaction, the filtrate was subjected to vapor diffusion of diethyl ether at room temperature in *air*, which resulted in small dark green crystals suitable for X-ray diffraction. Yield: 23 mg (32%). IR (neat, cm^{-1}): 1599 s, 1577 s, 1472 s, 1454 m, 1437 m, 1352 m, 1256 m, 1151 m, 1063 m, 896 w, 763 s, 709 m, 590 s, 433 m. High-resolution mass spectrometry (HR-MS) (ESI+): m/z 482.0328 $[M]^+$. UV/Vis in MeCN, λ_{max} (in nm) (ε in M^{-1} cm^{-1}): 563 (3730), 413 (5230), 340 (15 400), 292 (27 800), 245 (32 500). Anal. calcd for $C_{24}H_{18}FeIN_4S_2{\cdot}0.25I_2$: C 42.85, H 2.70, N 8.33%; found: C 43.14, H 2.92, N 8.41%.

[(NNS)$_2$Fe]. Under dinitrogen atmosphere, 50 mg (0.23 mmol) of **L1** was dissolved in 2 mL of MeCN, and 40 μL (0.23 mmol) of *N*,*N*-diisopropylethylamine was added. The mixture was stirred for 10 min. In a separate vial, FeI_2 (36 mg, 0.12 mmol) was dissolved in 2 mL of MeCN and then added to the solution. The resultant solution was stirred for 30 min at *room temperature*. The solvent was removed in vacuo, and the residue was washed with Et_2O, which afforded a dark green powder. Yield: 43 mg (76%). The dark green crystal suitable for X-ray diffraction was obtained from MeCN solution subjected to diethyl ether vapor diffusion. IR (neat, cm^{-1}): 1657 m, 1587 s, 1568 s, 1481 s, 1438 m, 1421 m, 1250 s, 1144 s, 1062 s, 1024 m, 909 m, 834 s, 759 s, 735 s, 654 s, 600 m, 439 s. UV/Vis in MeCN, λ_{max} (in nm) (ε in M^{-1} cm^{-1}): 614 (2210), 441 (5000), 319 (12 600), 281 (15 300).

In situ preparation of [(N^{Ph}NS^{DMPh})Fe(CO)$_2$(Br)] (8). Under dinitrogen atmosphere, 0.010 g (0.0245 mmol) of $\mathbf{L_B}$ was dissolved in 1 mL of THF as a pale yellow solution in a vial. Then, 3.65 μL (0.0245 mmol) of 1,8-diazabicyclo[5.4.0]undec-7-ene (DBU) was added to the same vial and stirred for 20 min. In a separate vial, 0.008 g (0.0245 mmol) of $[Fe(CO)_4(Br)_2]$ was dissolved in another 1 mL of THF to generate a dark red solution. At −30 °C, the addition of $[Fe(CO)_4(Br)_2]$ solution to the ligand solution immediately generated a dark green solution, which was stirred at −40 °C for 2 h. The resulting product was not stable. After the product was subjected to vapor diffusion of diethyl ether at −30 °C, dark green crystals suitable for X-ray diffraction were isolated, which proved to be $[(\mathbf{N^{Ph}NS^{DMPh}})_2\mathbf{Fe}]$ (**9**). The ^{13}C NMR spectrum of **8** was acquired with in situ synthesized product, and the J-Y tube was charged with CO gas and kept at −30 °C to avoid product decomposition. (***Caution!*** *Decomposition could lead to explosion, handle with care.*) IR for **8** (neat, cm^{-1}): 2036 m, 1985 m, 1643 s, 1581 m, 1441 m, 1321 m, 1206 w, 1063 m, 858 m, 775 m, 699 w. ^{13}C NMR (126 MHz, THF, −30 °C): δ = 215.2, 210.9, 166.4, 163.0, 155.7, 153.8, 145.5, 143.3, 140.8, 139.4, 137.1, 136.2, 131.4, 131.2, 130.5, 128.9, 128.8, 128.4, 127.8, 127.6, 127.1, 123.8, 109.9, 20.7, 20.4.

[(N^{Ph}NS^{DMPh})$_2$Fe] (9) (Method B). Under dinitrogen atmosphere, $\mathbf{L_B}$ (30 mg, 0.074 mmol) in 1 mL of PhF was mixed with *N*,*N*-diisopropylethylamine (7.0 μL, 0.040 mmol). In a separate vial, $FeBr_2$ (8.7 mg, 0.040 mmol) was dissolved in 1 mL of PhF and then was added to $\mathbf{L_B}$. The solution turned dark green immediately and was stirred for 1 h. The solvent was removed in vacuo, and the residue was washed with diethyl ether and pentane. The dark green crystals suitable for X-ray diffraction were obtained from PhF solution subjected to diethyl ether vapor diffusion at −30 °C. Yield: 21 mg (68%) IR (neat, cm^{-1}): 1582 m, 1471 m, 1436 s, 1422 m, 1324 m, 1308 m, 1275 m, 1228 m, 1153 w, 1128 w, 937 m, 743 s, 686 s, 643 s, 593 m. MS (ESI, m/z): 870 $[M]^+$.

Stability Studies. *Non-bulky Complexes.* In two separate vials, $[Fe(CO)_4(I)_2]$ and the specific NNS ligand were dissolved in MeCN, respectively. The solutions were cooled to −30 °C and then mixed together in the dark (the concentrations of product were ~0.5 mM). The resultant solution was immediately transferred to an air-free cuvette, and UV/vis spectra were acquired every 5 min.

Bulky Complexes. In two separate vials, $[Fe(CO)_4(I)_2]$ and $\mathbf{L_B}$ ligand were dissolved in THF, respectively (DBU was added to the ligand). The solutions were cooled to −30 °C and then mixed together in the dark (the concentrations of product were ~0.5 mM). The resultant solutions were immediately transferred to an air-free cell, and IR spectra were obtained at a rate of one per minute.

Physical Measurements. NMR spectra were collected on Varian 400 MHz spectrometer, and chemical shifts were referenced to

DOI: 10.1021/acs.inorgchem.8b01185
Inorg. Chem. XXXX, XXX, XXX−XXX

$CDCl_3$. Solid-state infrared spectra were recorded on a Bruker Alpha spectrometer equipped with a diamond attenuated total reflectance (ATR) crystal. Mass spectra (MS) were acquired on either Thermo Scientific TSQ (CI) or Thermo Finnigan TSQ with Dionex Ultimate 3000 LC (ESI). The UV/vis absorption spectra were obtained at 298 K with an Agilent Cary 60 spectrophotometer. Microanalytical (C, H, N) data were provided by Midwest Microlabs.

X-ray Diffraction Data Collection and Crystal Structure Refinement. The data for **1**, **2**, and **4** were collected on a Rigaku AFC12 diffractometer with a Saturn 724+ CCD using a Mo Kα radiation with graphite monochromator. Reduced temperatures were maintained using an Oxford Cryostream low-temperature device. Data reductions were performed using Rigaku CrystalClear version 1.4.0.[32] The data for **5**, **9**, and $[Fe(NNS)_2]$ were collected on an Agilent Technologies SuperNova Dual Source diffractometer using a μ-focus Cu Kα radiation (λ = 1.5418 Å) with collimating mirror monochromators. Data reduction was performed using Agilent Technologies CrysAlisPro 1.171.37.31.[33] Reduced temperatures were maintained using an Oxford Cryostream low-temperature device. Structures were solved by direct methods using SuperFlip[34] and refined by full-matrix least-squares on F^2 with anisotropic displacement parameters for the non-H atoms using SHELXL-2013.[35] Structure analysis was aided by PLATON98[36] and WinGX.[37] The hydrogen atoms on carbon were calculated in ideal positions with isotropic displacement parameters set to 1.2 × U_{eq} of the attached atom (1.5 × U_{eq} for methyl hydrogen atoms). The data were checked for secondary extinction effects, but no correction was necessary. Neutral atom scattering factors and values used to calculate the linear absorption coefficient are from the International Tables for X-ray Crystallography.

DFT Calculations. DFT calculations were performed for **1**, **4**, **5**, and **8** in Gaussian 09.[38] Geometry optimizations and energy calculations employed B3LYP[39,40] functional; SDD[41] basis set for Fe; LanL2DZ[42,43] basis set for iodine; and 6-311G(d,p)[44,45] basis set for C, H, N, O, S. Frequency calculations were performed for **1**, **4**, and **8** at the same level of theory as the optimizations. All frequency calculations showed no imaginary frequencies, and the wavenumbers were scaled by 0.964.[46] Time-dependent density functional theory (TDDFT[47,48]) calculations were executed for **1**, **4**, and **5** to study their excited states at the same level of theory as the optimizations. The effect of solvation was considered by performing polarizable continuum model (PCM):[49] MeCN as solvent, ε = 35.688. GaussView[50] was used for visualization and data analysis.

■ ASSOCIATED CONTENT

Supporting Information

The Supporting Information is available free of charge on the ACS Publications website at DOI: 10.1021/acs.inorgchem.8b01185.

^{1}H and ^{13}C NMR data, IR and UV/vis spectra, and DFT calculations of the products (PDF)

Accession Codes

CCDC 1837368−1837373 contain the supplementary crystallographic data for this paper. These data can be obtained free of charge via www.ccdc.cam.ac.uk/data_request/cif, or by emailing data_request@ccdc.cam.ac.uk, or by contacting The Cambridge Crystallographic Data Centre, 12 Union Road, Cambridge CB2 1EZ, UK; fax: +44 1223 336033.

■ AUTHOR INFORMATION

Corresponding Author

*E-mail: mrose@cm.utexas.edu.

ORCID

Michael J. Rose: 0000-0002-6960-6639

Notes

The authors declare no competing financial interest.

■ ACKNOWLEDGMENTS

This research was supported by the Robert A. Welch Foundation (F-1822), the American Chemical Society PRF program (53542-DN13), and the UT Austin College of Natural Sciences.

■ REFERENCES

(1) Santhanam, K. S. V.; Press, R. J.; Miri, M. J.; Bailey, A. V.; Takacs, G. A. *Introduction to Hydrogen Technology,* 2nd ed.; Wiley: Hoboken, NJ, 2017.

(2) Momirlan, M.; Veziroglu, T. Current Status of Hydrogen Energy. *Renewable Sustainable Energy Rev.* **2002**, *6* (1−2), 141−179.

(3) Zhang, F.; Zhao, P.; Niu, M.; Maddy, J. The Survey of Key Technologies in Hydrogen Energy Storage. *Int. J. Hydrogen Energy* **2016**, *41* (33), 14535−14552.

(4) Schilter, D.; Camara, J. M.; Huynh, M. T.; Hammes-Schiffer, S.; Rauchfuss, T. B. Hydrogenase Enzymes and Their Synthetic Models: The Role of Metal Hydrides. *Chem. Rev.* **2016**, *116* (15), 8693−8749.

(5) Evans, D. J.; Pickett, C. J. Chemistry and the Hydrogenases. *Chem. Soc. Rev.* **2003**, *32* (5), 268.

(6) Lubitz, W.; Ogata, H.; Rüdiger, O.; Reijerse, E. Hydrogenases. *Chem. Rev.* **2014**, *114* (8), 4081−4148.

(7) Shima, S.; Pilak, O.; Vogt, S.; Schick, M.; Stagni, M. S.; Meyer-Klaucke, W.; Warkentin, E.; Thauer, R. K.; Ermler, U. The Crystal Structure of [Fe]-Hydrogenase Reveals the Geometry of the Active Site. *Science* **2008**, *321* (5888), 572−575.

(8) Hiromoto, T.; Ataka, K.; Pilak, O.; Vogt, S.; Stagni, M. S.; Meyer-Klaucke, W.; Warkentin, E.; Thauer, R. K.; Shima, S.; Ermler, U. The Crystal Structure of C176A Mutated [Fe]-Hydrogenase Suggests an Acyl-Iron Ligation in the Active Site Iron Complex. *FEBS Lett.* **2009**, *583* (3), 585−590.

(9) Yang, X.; Hall, M. B. Monoiron Hydrogenase Catalysis: Hydrogen Activation with the Formation of a Dihydrogen, Fe−$H^{\delta-}\cdots H^{\delta+}$−O, Bond and Methenyl-$H_4MPT^+$ Triggered Hydride Transfer. *J. Am. Chem. Soc.* **2009**, *131* (31), 10901−10908.

(10) Chen, D.; Scopelliti, R.; Hu, X. Reversible Protonation of a Thiolate Ligand in an [Fe]-Hydrogenase Model Complex. *Angew. Chem., Int. Ed.* **2012**, *51* (8), 1919−1921.

(11) Finkelmann, A. R.; Senn, H. M.; Reiher, M. Hydrogen-Activation Mechanism of [Fe] Hydrogenase Revealed by Multi-Scale Modeling. *Chem. Sci.* **2014**, *5* (11), 4474−4482.

(12) Chen, D.; Scopelliti, R.; Hu, X. A Five-Coordinate Iron Center in the Active Site of [Fe]-Hydrogenase: Hints from a Model Study. *Angew. Chem., Int. Ed.* **2011**, *50* (25), 5671−5673.

(13) Shima, S.; Chen, D.; Xu, T.; Wodrich, M. D.; Fujishiro, T.; Schultz, K. M.; Kahnt, J.; Ataka, K.; Hu, X. Reconstitution of [Fe]-Hydrogenase Using Model Complexes. *Nat. Chem.* **2015**, *7* (12), 995−1002.

(14) Muthiah, K. A. T.; Durgaprasad, G.; Xie, Z.-L.; Williams, O. M.; Joseph, C.; Lynch, V. M.; Rose, M. J. Mononuclear Iron(II) Dicarbonyls Derived from NNS Ligands - Structural Models Related to a "Pre-Acyl" Active Site of Mono-Iron (Hmd) Hydrogenase. *Eur. J. Inorg. Chem.* **2015**, *2015* (10), 1675−1691.

(15) Durgaprasad, G.; Xie, Z.-L.; Rose, M. J. Iron Hydride Detection and Intramolecular Hydride Transfer in a Synthetic Model of Mono-Iron Hydrogenase with a CNS Chelate. *Inorg. Chem.* **2016**, *55* (2), 386−389.

(16) Xie, Z.-L.; Durgaprasad, G.; Ali, A. K.; Rose, M. J. Substitution Reactions of Iron(II) Carbamoyl-Thioether Complexes Related to Mono-Iron Hydrogenase. *Dalt. Trans.* **2017**, *46* (33), 10814−10829.

(17) Kerns, S. A.; Magtaan, A.-C.; Vong, P. R.; Rose, M. J. Functional Hydride Transfer by a Thiolate-Containing Model of Mono-Iron Hydrogenase Featuring an Anthracene Scaffold. *Angew. Chem., Int. Ed.* **2018**, *57* (11), 2855−2858.

(18) Carlson, L. J.; Welby, J.; Zebrowski, K. A.; Wilk, M. M.; Giroux, R.; Ciancio, N.; Tanski, J. M.; Bradley, A.; Tyler, L. A. Spectroscopic Differences between Heterocyclic Benzothiazoline, -Thiazole and Imine Containing Ligands and Comparison of the Co and Cu

DOI: 10.1021/acs.inorgchem.8b01185
Inorg. Chem. XXXX, XXX, XXX−XXX

Pyridine Benzothiazole and Imine Complexes. *Inorg. Chim. Acta* **2011**, *365* (1), 159−166.
(19) Lynn, M. A.; Carlson, L. J.; Hwangbo, H.; Tanski, J. M.; Tyler, L. A. Structural Influences on the Oxidation of a Series of 2-Benzothiazoline Analogs. *J. Mol. Struct.* **2012**, *1011*, 81−93.
(20) Lindoy, L. F. Reactions Involving Metal Complexes of Sulphur Ligands. *Coord. Chem. Rev.* **1969**, *4* (1), 41−71.
(21) Xu, H.-J.; Liang, Y.-F.; Cai, Z.-Y.; Qi, H.-X.; Yang, C.-Y.; Feng, Y.-S. CuI-Nanoparticles-Catalyzed Selective Synthesis of Phenols, Anilines, and Thiophenols from Aryl Halides in Aqueous Solution. *J. Org. Chem.* **2011**, *76* (7), 2296−2300.
(22) Fu, Y.; Wang, J.-Y.; Zhang, D.; Chen, Y.-F.; Gao, S.; Zhao, L.-X.; Ye, F. Solvent-Free Synthesis and Safener Activity of Sulfonylurea Benzothiazolines. *Molecules* **2017**, *22* (10), 1601.
(23) Plant, D.; Tarbell, D. S.; Whiteman, C. An Infrared Study of Hydrogen Bonding Involving the Thiol Group. *J. Am. Chem. Soc.* **1955**, *77* (6), 1572−1575.
(24) Noveron, J. C.; Herradora, R.; Olmstead, M. M.; Mascharak, P. K. Low-Spin Iron(III) Complexes with N, S Coordination: Syntheses, Structures, and Properties of Bis(N-2-Mercaptophenyl-2′-Pyridylmethyleniminato)Iron(III) Tetraphenylborate and Bis(N-2-Mercapto-2-Methylpropyl-2′-Pyridylmethyleniminato)Iron(III) Tetraphenylborate. *Inorg. Chim. Acta* **1999**, *285* (2), 269−276.
(25) Turrell, P. J.; Wright, J. A.; Peck, J. N. T.; Oganesyan, V. S.; Pickett, C. J. The Third Hydrogenase: A Ferracyclic Carbamoyl with Close Structural Analogy to the Active Site of Hmd. *Angew. Chem., Int. Ed.* **2010**, *49* (41), 7508−7511.
(26) Lyon, E. J.; Shima, S.; Boecher, R.; Thauer, R. K.; Grevels, F.-W.; Bill, E.; Roseboom, W.; Albracht, S. P. J. Carbon Monoxide as an Intrinsic Ligand to Iron in the Active Site of the Iron−Sulfur-Cluster-Free Hydrogenase H_2-Forming Methylenetetrahydromethanopterin Dehydrogenase As Revealed by Infrared Spectroscopy. *J. Am. Chem. Soc.* **2004**, *126* (43), 14239−14248.
(27) Li, B.; Liu, T.; Popescu, C. V.; Bilko, A.; Darensbourg, M. Y. Synthesis and Mössbauer Characterization of Octahedral Iron(II) Carbonyl Complexes $FeI_2(CO)_3L$ and $FeI_2(CO)_2L_2$: Developing Models of the [Fe]-H $_2$ Ase Active Site. *Inorg. Chem.* **2009**, *48* (23), 11283−11289.
(28) Shima, S.; Schick, M.; Kahnt, J.; Ataka, K.; Steinbach, K.; Linne, U. Evidence for Acyl−iron Ligation in the Active Site of [Fe]-Hydrogenase Provided by Mass Spectrometry and Infrared Spectroscopy. *Dalt. Trans.* **2012**, *41* (3), 767−771.
(29) Chen, D.; Scopelliti, R.; Hu, X. [Fe]-Hydrogenase Models Featuring Acylmethylpyridinyl Ligands. *Angew. Chem., Int. Ed.* **2010**, *49* (41), 7512−7515.
(30) Hieber, W.; Bader, G. Reaktionen Und Derivate Des Eisencarbonyls, II.: Neuartige Kohlenoxyd-Verbindungen von Eisenhalogeniden. *Ber. Dtsch. Chem. Ges. B* **1928**, *61* (8), 1717−1722.
(31) Lindoy, L. F.; Livingstone, S. E. The Metal-Ion Induced Rearrangement of 2-(2-Pyridyl)Benzothiazoline. *Inorg. Chim. Acta* **1967**, *1*, 365−370.
(32) *CrystalClear*, 1.4.0; Rigaku Americas Corporation: Woodlands, TX, 2008.
(33) *CrysAlisPro*, 1.171.37.31; Agilent Technologies UK Ltd.: Oxford, UK, 2013.
(34) Palatinus, L.; Chapuis, G. *SUPERFLIP* − a Computer Program for the Solution of Crystal Structures by Charge Flipping in Arbitrary Dimensions. *J. Appl. Crystallogr.* **2007**, *40* (4), 786−790.
(35) Sheldrick, G. M. A Short History of SHELX. *Acta Crystallogr., Sect. A: Found. Crystallogr.* **2008**, *64* (1), 112−122.
(36) Spek, A. L. Structure Validation in Chemical Crystallography. *Acta Crystallogr., Sect. D: Biol. Crystallogr.* **2009**, *65* (2), 148−155.
(37) Farrugia, L. J. *WinGX* Suite for Small-Molecule Single-Crystal Crystallography. *J. Appl. Crystallogr.* **1999**, *32* (4), 837−838.
(38) Frisch, M. J.; Trucks, G. W.; Schlegel, H. B.; Scuseria, G. E.; Robb, M. A.; Cheeseman, J. R.; Scalmani, G.; Barone, V.; Petersson, G. A.; Nakatsuji, H.; et al. *Gaussian 09,* Revision A.02; Gaussian, Inc.: Wallingford, CT, 2009.
(39) Becke, A. D. Density-functional Thermochemistry. III. The Role of Exact Exchange. *J. Chem. Phys.* **1993**, *98* (7), 5648−5652.
(40) Stephens, P. J.; Devlin, F. J.; Chabalowski, C. F.; Frisch, M. J. Ab Initio Calculation of Vibrational Absorption and Circular Dichroism Spectra Using Density Functional Force Fields. *J. Phys. Chem.* **1994**, *98* (45), 11623−11627.
(41) Dolg, M.; Wedig, U.; Stoll, H.; Preuss, H. Energy-adjusted Ab Initio Pseudopotentials for the First Row Transition Elements. *J. Chem. Phys.* **1987**, *86* (2), 866−872.
(42) Hay, P. J.; Wadt, W. R. *Ab Initio* Effective Core Potentials for Molecular Calculations. Potentials for the Transition Metal Atoms Sc to Hg. *J. Chem. Phys.* **1985**, *82* (1), 270−283.
(43) Hay, P. J.; Wadt, W. R. *Ab Initio* Effective Core Potentials for Molecular Calculations. Potentials for K to Au Including the Outermost Core Orbitals. *J. Chem. Phys.* **1985**, *82* (1), 299−310.
(44) Krishnan, R.; Binkley, J. S.; Seeger, R.; Pople, J. A. Self-consistent Molecular Orbital Methods. XX. A Basis Set for Correlated Wave Functions. *J. Chem. Phys.* **1980**, *72* (1), 650−654.
(45) McLean, A. D.; Chandler, G. S. Contracted Gaussian Basis Sets for Molecular Calculations. I. Second Row Atoms, Z = 11−18. *J. Chem. Phys.* **1980**, *72* (10), 5639−5648.
(46) National Institute of Standards and Technology. Computational Chemistry Comparison and Benchmark DataBase. https://cccbdb.nist.gov/vibscalejust.asp (accessed Apr 26, 2018).
(47) Gross, E. K. U.; Kohn, W. Time-Dependent Density-Functional Theory. *Adv. Quantum Chem.* **1990**, *21*, 255−291.
(48) Gross, E. K. U.; Dobson, J. F.; Petersilka, M. Density Functionals: Theory and Applications. In *Springer Series Topics in Current Chemistry;* Nalewajski, R. F., Ed.; Springer: Heidelberg, Germany, 1996; Vol. *81*, p 81.
(49) Tomasi, J.; Mennucci, B.; Cammi, R. Quantum Mechanical Continuum Solvation Models. *Chem. Rev.* **2005**, *105* (8), 2999−3094.
(50) Dennington, R.; Keith, T.; Millam, J. *GaussView,* Version 5; Semichem Inc.: Shawnee Mission, KS, 2009.

DOI: 10.1021/acs.inorgchem.8b01185
Inorg. Chem. XXXX, XXX, XXX−XXX